molecules

MDPI

Article

Zero-Waste Hydrogel Design via Integral Biomass Valorization of Protein-Rich Spirulina Microalgae

Leandro L. Aquino [1], Samara C. Silva-Pituco [1], Alejandro Hernandez-Sosa [2], Elsa C. Ramalhosa [1], Rebeca Hernandez [2], Eliane Colla [3], Arantzazu Santamaria-Echart [1,*] and Maria F. Barreiro [1,*]

[1] CIMO, LA SusTEC, Instituto Politécnico de Bragança, Campus de Santa Apolónia, 5300-253 Bragança, Portugal; leandroaquino@ipb.pt (L.L.A.); samaras@ipb.pt (S.C.S.-P.); elsa@ipb.pt (E.C.R.)

[2] Instituto de Ciencia y Tecnología de Polímeros (ICTP), CSIC, c/Juan de la Cierva, 3, 28006 Madrid, Spain; alejandrohs@ictp.csic.es (A.H.-S.); rhernandez@ictp.csic.es (R.H.)

[3] Programa de Pós-graduação em Tecnologia de Alimentos (PPGTA), Departamento Acadêmico de Alimentos (DAALM), Universidade Tecnológica Federal do Paraná, Câmpus Medianeira, Paraná 85884-000, Brazil; ecolla@utfpr.edu.br

* Correspondence: asantamaria@ipb.pt (A.S.-E.); barreiro@ipb.pt (M.F.B.)

Abstract

Interest in alternative protein sources has grown, with Spirulina, a microalga belonging to the genus *Limnospira* (formerly *Arthrospira*), emerging as a key option. Guided by sustainability principles, this study explored the gelling capacity and hydrogel-forming properties of integral Spirulina biomass (SpB), targeting applications in structured foods. Two experimental designs (DoE) were employed. One to identify key factors influencing hydrogel formation, and another to optimize the formulation (22 wt%, pH 5.6, thermal gelation at 90 °C). Syneresis analysis revealed that high SpB hydrogels experienced less water loss, with the 22% sample losing just 2.51% after 14 days, due to its dense, particulate morphology as observed by means of scanning electron microscopy. Rheological analysis confirmed the optimized formulation's superior mechanical properties, with a storage modulus (G′) 24-times higher than the low concentration reference sample (~1890 Pa), remaining dominant over the loss modulus (G″) (G′ > G″) across the analysed frequency range, corroborating a strong elastic behaviour. Although the recovery tests showed partial recovery (27.1%) after high shear, the high residual stiffness (≈515 Pa) confirmed the material's ability to maintain its shape. These results enabled successful 3D printing tests with the optimized hydrogel, pointing out its potential for innovative food applications in structured food design.

Keywords: Spirulina; protein-rich biomass; microalgal hydrogels; technological properties; 3D printing

Academic Editor: Li-Ming Zhang

Received: 31 December 2025
Revised: 31 January 2026
Accepted: 3 February 2026
Published: 9 February 2026

1. Introduction

The consumption of protein-rich healthy foods has grown significantly, driven by population growth and increased concern for healthier lifestyles. This demographic pressure demands alternative, sustainable production approaches that reduce land use, minimize environmental impact, and favour efficient practices, in opposition to extensive livestock practices [1]. In this context, microalgae are positioned as an attractive alternative due to their lower greenhouse gas emissions and reduced land use and freshwater consumption per gram of produced protein [2]. The strategy of integrated processing and revalorization

of microalgae biomass is vital in achieving sustainability goals and aligning with circular economy principles [3–5]. In this perspective, approaches focused on green growth and the generation of value-added products from total biomass are increasingly being adopted globally [6].

Microalgae are mostly eukaryotic, photosynthetic unicellular microorganisms, while cyanobacteria, one of the earliest forms of life on Earth, are prokaryotic microorganisms included as microalgae due to their similar physiological characteristics [7]. Historically, the consumption and use of microalgae and cyanobacteria date back to the Aztec people in Mexico, who harvested these organisms and incorporated them into their diet [8,9]. Recently, algae and microalgae have emerged as viable alternatives to common protein sources, offering an excellent amino acid profile and providing polyunsaturated fatty acids, vitamins, minerals, antioxidants, and dietary fibres [10–12].

One of the most notable species of microalgae is Spirulina (*Limnospira platensis*, formerly *Arthrospira platensis*) [13], a cyanobacterium known for its high protein content [14], which typically accounts for 50–70% of its dry weight and can reach 60–70% in certain cases [15–17]. In its composition, it contains phycobiliproteins, pigments that act as photosynthetic pigments for the organism. Among these, phycocyanin is of industrial interest due to its striking blue coloration and its proven anti-inflammatory and antioxidant properties [18]. Other important compounds include lipids and carbohydrates, which constitute approximately 6–13% and 15–25% dry basis, respectively, with carbohydrates serving essential functions in energy storage and in preserving cellular structural integrity [19].

Proteins, alongside carbohydrates, are of great interest for food applications due to their nutritional value and technological properties, including gelling capacity. Consequently, microalgae are positioned as highly promising sources for the development of gels as functional food matrices [20–23]. This approach aligns with the growing need to design plant-based foods in which biopolymer gelation is engineered for enhanced texture and functionality [24]. Given this context, ongoing research in protein-rich algae is focused on leveraging innovations in protein extraction and modification to maximize their techno-functional performance and drive sustainable food applications [25].

The availability of microalgae on the market remains limited, with most commercialization occurring in powder or tablet form for food supplements [26], with *L. platensis* among the most representative examples. Extracted *L. platensis* proteins have been characterized for their technological functionalities, demonstrating excellent emulsifying, foaming, and water/oil absorption capacities, which have drawn interest in their use in complex food systems [27,28]. In this context, Silva Faresin et al. [29] developed functional ice creams with reduced fat (50%) and sugar (25%) content, incorporating functional ingredients such as inulin, Spirulina, and a phycocyanin extract, while maintaining sensory characteristics. Dinçoğlu et al. [30] used *L. platensis* as an additive in yogurts, which significantly impacted the quality characteristics and exhibited potent prebiotic properties. Furthermore, Spirulina powder has been successfully used to enrich ricotta cheese, improving its textural properties, enhancing its nutritional content (protein, fat, ash, and fibre), and improving its visual appeal [31].

Microalgae-based hydrogels often involve the extraction and purification of specific biopolymers, such as phycobiliproteins or polysaccharides. However, these conventional extraction methods are typically energy-intensive and often require the use of chemical solvents, which not only increase the cost and complexity of the formulation but also generate substantial amounts of residual biomass waste [32]. In contrast, the use of the whole biomass, a "zero-waste" strategy, maximizes the raw material's value by valuing the complete profile of its inherent gelling components (proteins, carbohydrates), enhancing nutritional value. This holistic approach offers significant energy and cost savings by

bypassing purification steps and eliminating solvent consumption [33]. Furthermore, using the entire biomass and avoiding extractions preserves the full nutritional and functional matrix, including minerals, antioxidants, and fibers, which are often lost in refined extracts [34]. This preservation promotes a synergistic effect within the hydrogel structure, enhancing its techno-functional performance while aligning the material development directly with the principles of the circular economy and sustainability within food and material applications [35].

In this context, this work employs the entire Spirulina biomass (SpB) to develop hydrogels. Hydrogel formation was achieved through a simple, cost-effective two-step process that includes, first, mechanical treatment to disrupt the microalgal cell wall, promoting the release of internal biopolymers (e.g., proteins and carbohydrates), followed by a thermal treatment step to induce physical cross-linking. An experimental design strategy (DoE) was applied, initially using a fractional factorial design 2^{6-2} to screen for the most influential variables in hydrogel formation. Then, a central composite rotatable design 2^2 was used to address the most relevant variables and achieve optimal conditions for forming a hydrogel from SpB. The experimental designs were characterized and optimized to maximize the hydrogel quality based on key response variables, namely, firmness, cohesiveness, cohesion, and work of cohesion obtained from textural tests, which are essential for determining the structural rigidity and printability potential. Given the increasing demand for complex food structures that can support customized nutrition, rheological behaviour, and the material's 3D printability, these technological properties were evaluated. Therefore, the microstructure of the optimized hydrogels was characterized, and comprehensive rheology and 3D printing tests were performed to validate the material's suitability for additive manufacturing in the food sector.

2. Results and Discussion

2.1. Hydrogel-Forming Process

2.1.1. Initial Screening

The initial screening process to determine the minimum concentration required for hydrogel formation is illustrated in Figure 1. Tests conducted at low SpB concentrations of 2, 6, and 12 wt% using the inverted-tube method showed no gelation, as the samples flowed through the vial, indicating that the solutions remained in the fluid or dilute state. At higher SpB concentrations, the inverted-tube test became positive, indicating successful gel formation. Specifically, at 16 wt% concentration, fluid flow through the vial was significantly reduced. A completely stationary, self-supporting behaviour characteristic of a robust gel was clearly observed at 20 wt% biomass concentration.

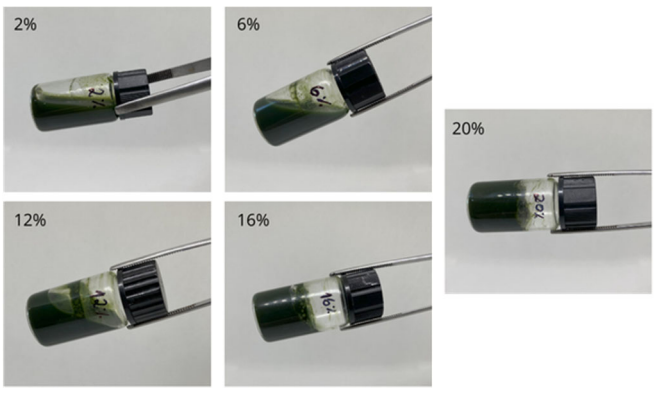

Figure 1. Preliminary tests on gel formation using different Spirulina biomass concentrations (2–20 wt%).

These preliminary results established that a minimum threshold concentration of SpB (12–16 wt%) is required to form a physically cross-linked network capable of resisting gravitational flow. Consequently, the subsequent experimental design focused on optimizing conditions above this critical concentration range to improve the hydrogel's properties.

2.1.2. Identification of the Significant Variables in Hydrogel Formation

The hydrogel formation studies were planned using a fractional factorial design (FFD) 2^{6-2}, with the biomass concentration in the range 12–20 wt%. The experimental runs and the textural responses to evaluate the influence of the gel-forming conditions are summarized in Table 1.

Table 1. Fractional factorial design (FFD) 2^{6-2} matrix with coded and real values of the independent variables (x_1–x_6) and response variables (y_1–y_4) for the formation of hydrogels.

Runs	x_1	x_2	x_3	x_4	x_5	x_6	y_1	y_2	y_3	y_4
1	−1 (85)	−1 (6)	−1 (30)	−1 (5)	−1 (9500)	−1 (12)	16.28	268.53	−7.81	−2.42
2	1 (95)	−1 (6)	−1 (30)	−1 (5)	1 (9500)	−1 (12)	25.11	322.81	−7.02	−2.12
3	−1 (85)	1 (10)	−1 (30)	−1 (5)	1 (9500)	1 (20)	82.27	1345.99	−87.21	−147.85
4	1 (95)	1 (10)	−1 (30)	−1 (5)	−1 (6500)	1 (20)	105.61	1738.54	−108.40	−179.17
5	−1 (85)	−1 (6)	1 (60)	−1 (5)	1 (9500)	1 (20)	150.18	2644.72	−143.69	−239.43
6	1 (95)	−1 (6)	1 (60)	−1 (5)	−1 (6500)	1 (20)	110.40	1793.53	−108.22	−173.83
7	−1 (85)	1 (10)	1 (60)	−1 (5)	−1 (6500)	−1 (12)	32.38	533.86	−23.38	−32.78
8	1 (95)	1 (10)	1 (60)	−1 (5)	1 (9500)	−1 (12)	27.07	467.61	−21.86	−29.43
9	−1 (85)	−1 (6)	−1 (30)	1 (15)	−1 (6500)	1 (20)	99.68	1842.14	−119.07	−206.22
10	1 (95)	−1 (6)	−1 (30)	1 (15)	1 (9500)	1 (20)	194.77	3425.20	−170.98	−256.17
11	−1 (85)	1 (10)	−1 (30)	1 (15)	1 (9500)	−1 (12)	26.52	463.50	−27.33	−39.44
12	1 (95)	1 (10)	−1 (30)	1 (15)	−1 (6500)	−1 (12)	54.57	826.50	−36.59	−64.30
13	−1 (85)	−1 (6)	1 (60)	1 (15)	1 (9500)	−1 (12)	95.39	1566.60	−83.35	−118.96
14	1 (95)	−1 (6)	1 (60)	1 (15)	−1 (6500)	−1 (12)	55.49	945.12	−44.22	−68.96
15	−1 (85)	1 (10)	1 (60)	1 (15)	−1 (6500)	1 (20)	59.29	1021.12	−66.21	−115.09
16	1 (95)	1 (10)	1 (60)	1 (15)	1 (9500)	1 (20)	57.65	966.54	−63.78	−109.85
17	0 (90)	0 (8)	0 (45)	0 (10)	0 (8000)	0 (16)	78.80	1275.80	−78.73	−115.05
18	0 (90)	0 (8)	0 (45)	0 (10)	0 (8000)	0 (16)	89.50	1391.36	−73.85	−116.25
19	0 (90)	0 (8)	0 (45)	0 (10)	0 (8000)	0 (16)	108.80	1909.17	−91.52	−155.55

x_1: Temperature (°C); x_2: pH; x_3: Heating time (min); x_4: Stirring time (min); x_5: Stirring speed (rpm); x_6: Biomass concentration (%); y_1: Firmness (g); y_2: Consistency (g·s); y_3: Cohesiveness (g); y_4: Work of cohesion (g·s).

The effect of the six independent process variables on the responses of firmness, consistency, cohesiveness, and work of cohesion was analysed, and the results are presented in Table S1 in the Supplementary Material.

The variables that significantly affected firmness and consistency ($p \leq 0.05$) were pH (x_2) and biomass concentration (x_6). The effect of pH was negative over the studied range (Table S1), indicating that lower pH values led to hydrogels with higher firmness and consistency. This behaviour can be explained by the fact that pH strongly influences the surface charge of SpB biomolecules, particularly proteins and polysaccharides. At lower pH values, electrostatic repulsion between polymer chains is reduced [36], favouring closer molecular interactions. Consequently, the gel matrix becomes more compact and aggregated, leading to improved firmness and consistency.

The biomass concentration (x_6) showed a positive effect, meaning that increasing the SpB content significantly favoured the firmness and consistency of the hydrogels. This confirms that the mechanical properties of a hydrogel can be directly controlled by changing the polymer concentration and/or the crosslink density [37]. In line with this observation, the higher concentration increased the total solids available for network formation, increasing the number of biomolecules capable of participating in intermolecular

interactions. This mechanism resulted in improved structural stability and enhanced water retention. Therefore, the combined effects of pH (molecular interactions) and biomass concentration (availability of solid material) are crucial determinants of the hydrogels' final mechanical properties.

Since cohesiveness and work of cohesion are determined from the negative area of the texture profile, the interpretation of the variable effects was inverted. Accordingly, the cohesiveness of the hydrogels increased with higher biomass concentration or lower pH. Higher cohesiveness indicated that the gel network became more resistant to rupture and tended to recover its integrity after deformation, resulting in a more elastic matrix.

For work of cohesion, biomass concentration (x_6) had a significant positive effect, with a positive trend. A greater degree of cohesion implied that more energy was required to disrupt the hydrogel's internal structure, indicating the formation of a denser network. This feature can improve water retention, reduce disintegration, and enhance mechanical stability. These attributes can be particularly advantageous for food products with a chewier texture or for biomedical and cosmetic applications requiring stronger, longer-lasting structural integrity.

2.1.3. Optimization of Hydrogel Formulation

Following the identification of pH and biomass concentration as the significant variables affecting the hydrogel formation process, a central composite rotatable design 2^2 was conducted to determine the optimal hydrogel formulation. The other non-significant variables from the FFD were fixed at the central point levels: the temperature was set at 90 °C, the heating time at 30 min, the stirring time at 10 min, and the stirring speed at 8000 rpm. The experimental matrix, including the real and coded values for the two variables and the corresponding textural responses, is presented in Table 2.

Table 2. Composite central rotational design (CCRD) 2^2 matrix with real and coded values of variables for the formation of hydrogels.

Runs	x_1	x_2	y_1	y_2	y_3	y_4
1	−1 (5.30)	−1 (16.90)	105.26	1757.94	−60.33	−78.17
2	1 (6.70)	−1 (16.90)	74.82	1281.03	−64.84	−115.08
3	−1 (5.30)	1 (21.10)	130.08	2372.33	−119.57	−217.67
4	1 (6.70)	1 (21.10)	122.15	2197.15	−104.45	−187.25
5	−1.41 (5.00)	0 (19.00)	112.07	1976.11	−100.08	−166.60
6	1.41 (7.00)	0 (19.00)	84.78	1352.18	−83.13	−124.73
7	0 (6.00)	−1.41 (16.00)	62.48	986.04	−30.98	−46.21
8	0 (6.00)	1.41 (22.00)	152.19	2520.06	−142.40	−208.07
9	0 (6.00)	0 (19.00)	121.66	2148.93	−99.97	−163.34
10	0 (6.00)	0 (19.00)	115.76	2038.54	−94.50	−157.03
11	0 (6.00)	0 (19.00)	119.76	2192.85	−111.77	−188.20

x_1: pH; x_2: Biomass concentration (%); y_1: Firmness (g); y_2: Consistency (g·s); y_3: Cohesiveness (g); y_4: Work of cohesion (g·s).

The analysis of variance (ANOVA), with non-significant parameters incorporated into the residues, for the composite central rotational design (CCRD) models summarized in Table S2 in the Supplementary Materials, showed that all models were highly significant ($p \leq 0.05$) and provided a good fit to the experimental data, with R^2 values ranging from 89.02% to 93.02%. This confirms that the response surfaces can reliably represent the hydrogel-forming process. The regression coefficients for the linear, quadratic, and interaction terms are detailed in Table S3 in the Supplementary Material. Mathematical models were developed for the four responses (firmness, consistency, cohesion, and work of cohesion), with the respective significant variables. The models developed to

predict the firmness and consistency of the hydrogel based on the significant independent ($p \leq 0.05$) variables (x_1: pH; x_2: biomass concentration (wt%)) within the studied ranges, and re-parameterized considering the non-statistically significant parameters incorporated into the residues, are shown in Equations (1) and (2):

$$Y_1\ (\text{Firmness}) = 119.06 - 9.62x_1 - 9.02x_1^2 + 24.88x_2 - 4.56x_2^2 \quad (1)$$

$$Y_2\ (\text{Consistency}) = 2126.77 - 191.81x_1 - 182.94x_1^2 + 462.49x_2 - 138.48x_2^2 \quad (2)$$

The response surfaces and contour plots (Figure 2a–d) show that firmness increased progressively with the biomass concentration, reaching a maximum around 22 wt%. pH presented a negligible effect on firmness, although values around 5.6 slightly favour the gel structure. For consistency, a clear pattern emerged: high biomass concentrations combined with a pH around 5.6 yielded the highest values. This fact indicates that the combined effects of pH and biomass enable simultaneous control of the hydrogel's texture and rigidity, which is critical for applications requiring mechanical stability, such as encapsulation systems, food matrices, and 3D-printed structures, where shape maintenance during and after deposition is essential.

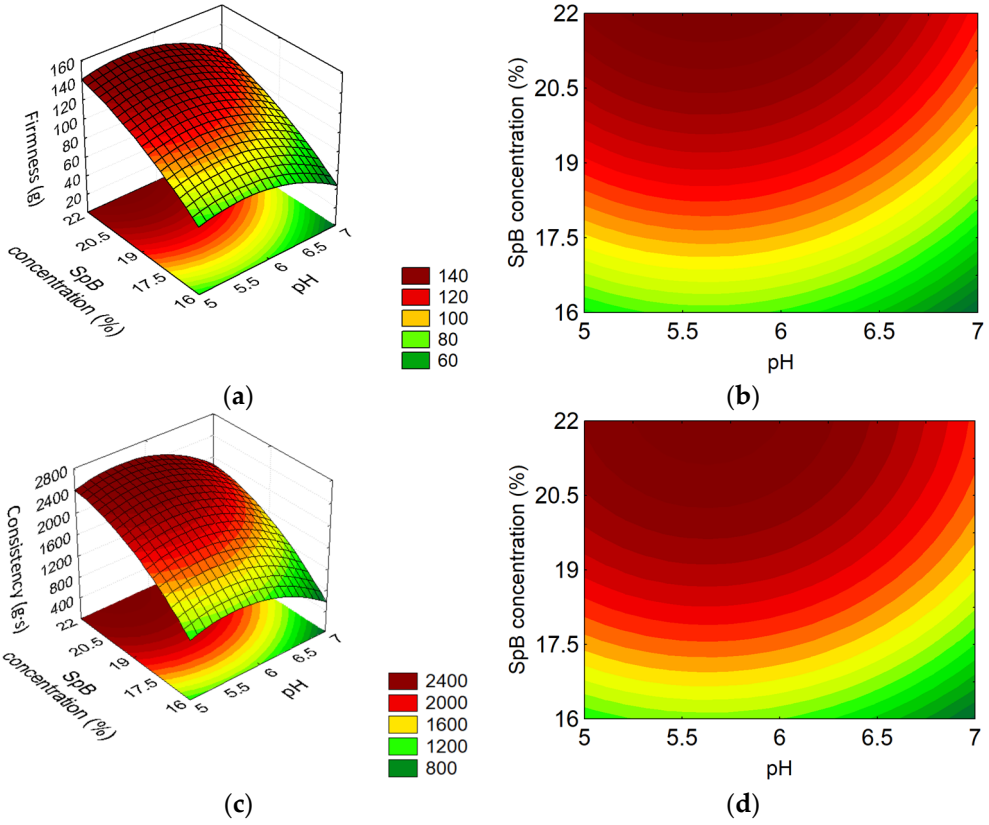

Figure 2. Response surfaces (**a**,**c**) and contour plots (**b**,**d**) for firmness (g) (Y_1), consistency (g·s) (Y_2) as a function of pH (x_1) and biomass concentration (wt%) (x_2) of the hydrogels, respectively.

Similarly, models for cohesiveness and work of cohesion were built considering only biomass concentration, since the pH (x_1) was not statistically significant ($p > 0.05$) for these two responses (Table S3). The resulting re-parameterized models are represented in Equations (3) and (4):

$$Y_3\ (\text{Cohesiveness}) = 96.72 + 32.05x_2 - 6.48x_2^2 \quad (3)$$

$$Y_4\ (\text{Work of cohesion}) = 161.92 + 55.07x_2 - 15.72x_2^2 \quad (4)$$

The surfaces (Figure 3a–d) indicated that both properties increased with biomass concentration, reaching a plateau at about 22 wt%. This plateau is considered the limit of hydrogel formation capacity due to the difficulty of fully solubilizing the total biomass. This behaviour is essential for applications requiring stable hydrogels, allowing formulation adjustments for different functions without compromising other physical properties, including in 3D printing, where gel flowability and shape retention are critical.

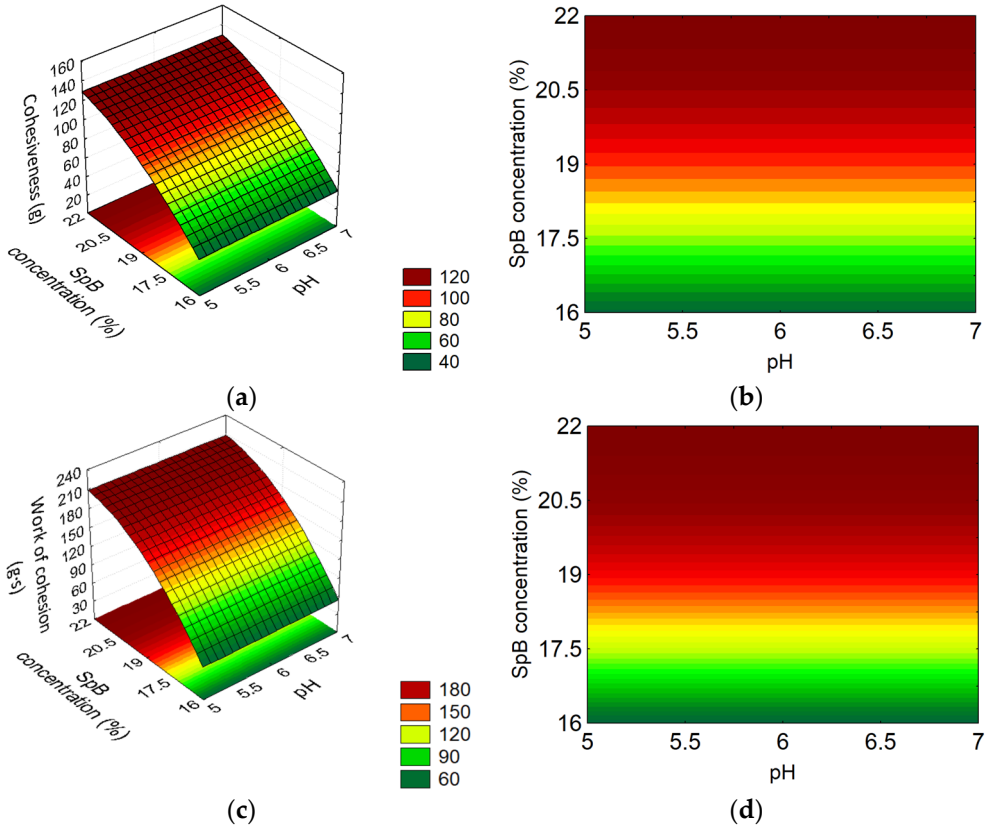

Figure 3. Response surfaces (**a**,**c**) and contour plots (**b**,**d**) for cohesiveness (g) (Y_3), work of cohesion (g·s) (Y_4) as a function of pH (x_1) and biomass concentration (wt%) (x_2) of the hydrogels, respectively.

In summary, the analysis of the response surfaces indicated that biomass concentration is the primary variable affecting all texture and cohesion properties. At the same time, pH plays a secondary but relevant role in maximizing consistency. Understanding these effects is essential for designing hydrogels with specific firmness, consistency, and cohesiveness profiles, adaptable to applications such as 3D printing of food or biomaterial structures, encapsulation of bioactive compounds, and structural supports.

2.2. Syneresis of Hydrogels

The syneresis of the samples formulated according to the experimental design was measured at 1, 7, and 14 days, corresponding to the CCRD experimental runs 1–11, as reported in Table 2, and shown in Figure 4. Runs 9, 10, and 11 were performed as independent experimental replicates at the central point. It is known that the syneresis varied over time due to the stabilization of the molecular interactions resulting from the gelling process [38].

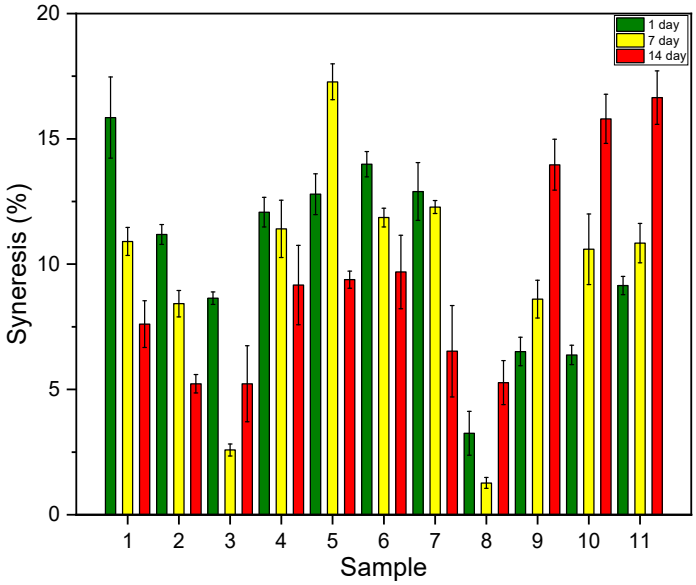

Figure 4. Effect of time on the syneresis of SpB hydrogels for the CCRD 2^2 samples (runs 1–11, as reported in Table 2).

The lowest syneresis values were observed for samples 3 and 8, which corresponded to the formulations with the highest biomass concentrations. This inverse relationship aligns with findings in protein-polysaccharide composite hydrogels, where high biopolymer concentration directly reinforces structural stability, leading to superior water-holding capacity and reduced syneresis [39]. Mechanistically, high concentrations of macromolecular components reduce molecular mobility within the network, reinforcing the hydrogel's structural stability and limiting syneresis over time.

Based on the cumulative characterization (namely, DoE's, texture profile analysis (TPA), and syneresis analysis), which confirmed the stability of the more concentrated samples, two formulations were selected for subsequent advanced testing. The 22 wt% formulation was chosen because it represented the optimized condition (22 wt% biomass at pH 5.6), offering superior mechanical performance (e.g., highest firmness and consistency) and highest stability (lowest syneresis). Moreover, the 12 wt% biomass formulation (near the critical minimum concentration) was retained as a crucial low-concentration comparative control to clearly demonstrate the impact of the network density on the final hydrogel performance.

2.3. Hydrogel Microstructure

The surface morphology of the 22 wt% SpB hydrogels at different magnifications is shown in Figure 5. Images A and B revealed a homogeneous, rough, and irregular surface, characterized by a network of interconnected aggregates. This suggests the formation of a particulate hydrogel, where protein constituents, potentially alongside other biomass components, self-assemble and aggregate into larger, distinct microstructures. This appearance was further detailed in the C and D images, which highlighted the coarsely aggregated particles that formed the bulk hydrogel. These larger structures demonstrated protein aggregation, but with a seemingly lower degree of cohesion, resulting in a porous, somewhat fragmented network.

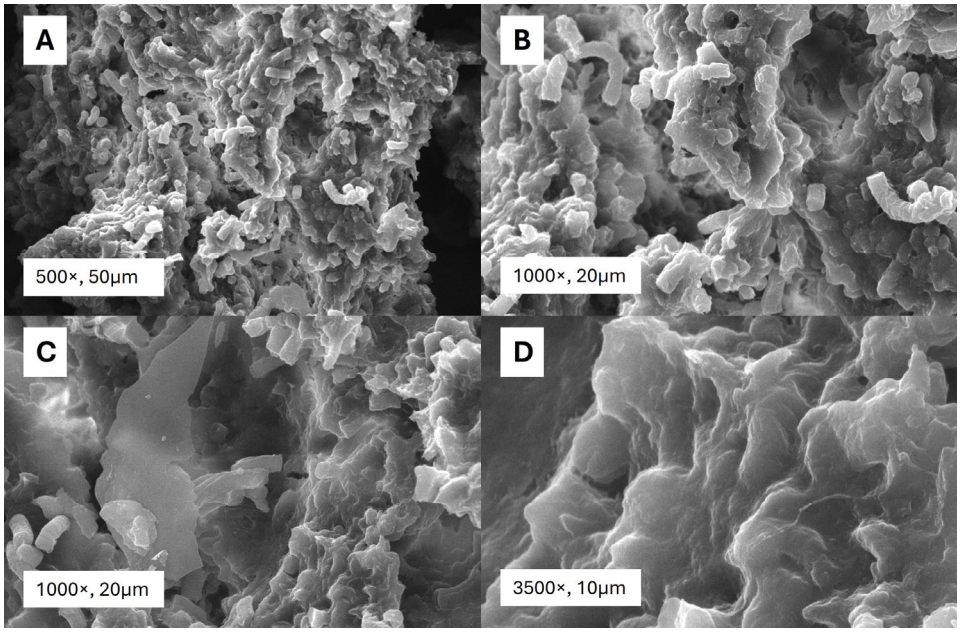

Figure 5. Scanning electron micrographs of Spirulina biomass hydrogel at different magnifications: (**A**) 500×, scale 50 µm; (**B**,**C**) 1000×, scale 20 µm; and (**D**) 3500×, scale 10 µm.

Similar particulate structures and aggregation patterns have been reported in the literature for other protein-based systems, such as whey protein hydrogels at pH 5.2 [40]. In those studies, the formulations also yielded particulate hydrogels composed of coarsely aggregated particles, demonstrating that the proteins aggregated into larger structures with less cohesion. The observations of this work are consistent with this mechanism, indicating that the SpB proteins, likely in conjunction with the carbohydrate components inherent to the biomass, formed a similar aggregated network structure under the established conditions. The presence of other biomass components might further contribute to the observed heterogeneity and the formation of these distinct aggregated domains, potentially influencing the overall mechanical properties and stability of the hydrogel.

2.4. Rheological Properties of Hydrogels

Figure 6 presents the flow curve tests, which determine the viscosity and shear stress of the hydrogels as a function of the shear rate. These tests are essential to confirm the rheological behaviour of the materials under flow conditions. The hydrogels demonstrated clear non-Newtonian behaviour, specifically exhibiting pseudoplasticity (shear-thinning), as the apparent viscosity decreased sharply with increasing shear rate [41]. This pseudoplastic behaviour is highly desirable for processing techniques, such as extrusion or 3D printing, since it allows the material to easily flow under stress (shear) while promptly recovering its structure after the stress is removed (essential for shape retention).

The hydrogel produced under the optimized conditions (22 wt% SpB) exhibited a significantly higher apparent viscosity than the sample made with the lowest concentration (12 wt% SpB), due to the higher solids' concentration. This difference confirmed that increasing biomass concentration led to a denser, more interconnected network structure, providing greater resistance to flow. Other studies developing bio-inks for 3D printing have shown similar results. For example, Wang et al. [42] also observed pseudoplastic behaviour and good printability when developing bio-inks from SpB residues. This behaviour is consistent with the rheological properties of the hydrogel, which demonstrated the necessary characteristics for controlled extrusion.

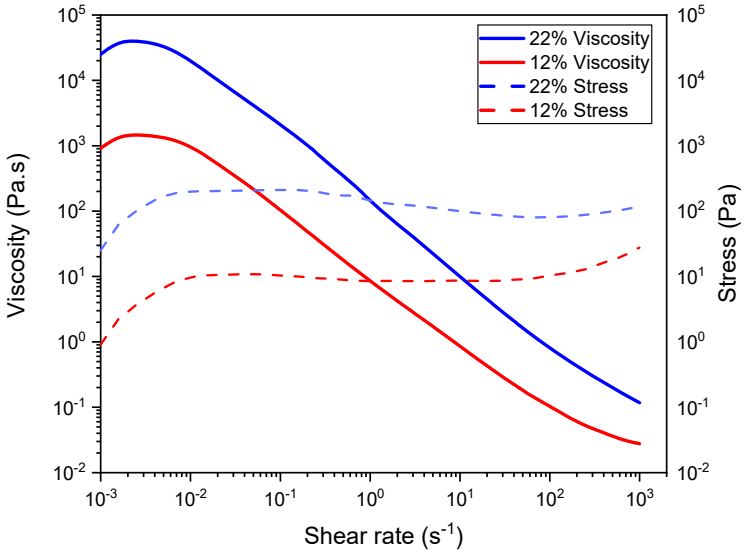

Figure 6. Flow test as a function of the shear rate of SpB hydrogels containing 12 and 22 wt% of biomass produced at pH 5.6.

Oscillatory tests (specifically amplitude or strain sweeps) were performed to assess the mechanical stability of the hydrogels by measuring the storage modulus (G′) and the loss modulus (G″) as a function of applied strain at a constant angular frequency. Figure 7 illustrates the results of the performed oscillation test by varying the strain amplitude at a constant angular frequency of 10^{-1} Hz.

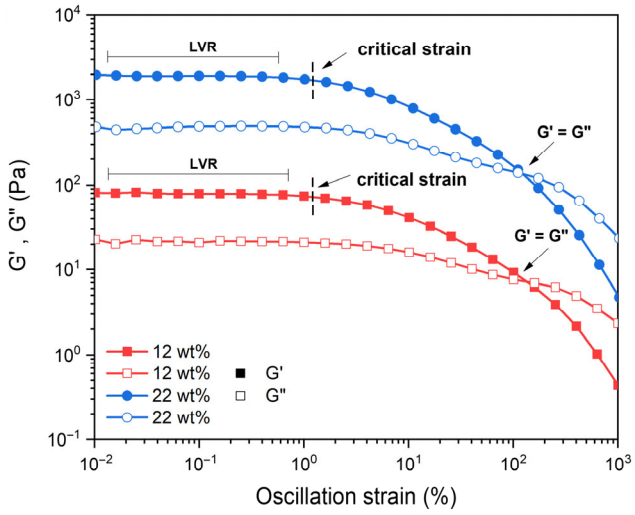

Figure 7. Strain sweeps at a constant frequency (10^{-1} Hz) of SpB hydrogel of 12 wt% and 22 wt% biomass produced at pH 5.6.

Amplitude-sweep tests (Figure 7) confirmed the strong viscoelastic gel behaviour of both samples (G′ > G″ throughout the linear viscoelastic region (LVR)). However, the G′ data revealed that γc, defined as the 95% drop in G′, was relatively low and similar across both hydrogels, ranging from 0.4% to 0.6%. This low, similar γc suggested that the initial mechanism of structural yielding is the same at both concentrations, dominated by weak physical forces, such as hydrogen bonds, that are easily overcome by small stresses.

Despite this similar limitation in the LVR, the hydrogels showed significant differences in overall mechanical performance. The 22 wt% hydrogel showed a mean G′ of ~1890 Pa in the LVR, which is over 24× higher than the 78.5 Pa observed for the 12 wt% hydrogel. This stiffness confirmed that the 22 wt% formulation established a significantly more rigid

network, attributed to the higher protein and carbohydrate content, which contribute to the formation of hydrogel structures [43]. Although limited solubility and suboptimal techno-functional properties remain key challenges for using plant proteins in food formulations [39], modulating protein aggregation and thereby reinforcing the gel network via pH control is a common strategy in protein/polysaccharide systems to achieve superior mechanical properties [44].

The storage modulus of the 22% SpB hydrogel (~1890 Pa) demonstrates a high structuring efficiency when compared to other Spirulina-based systems. For example, Wang et al. [42] developed 3D printing inks from Spirulina residues and found that, even with a significant reduction in moisture content, the G′ values remained within a similar range to those of our integral hydrogel. Specifically, their Spirulina residues inks with 25% and 20% moisture exhibited G′ values of approximately 1600 Pa and 3000 Pa, respectively. The fact that our 22% SpB hydrogel achieves ~1900 Pa while maintaining a much higher water content (~78%) suggests that the integral biomass approach preserves a more effective network of native proteins and polysaccharides. This native matrix can sustain a gel structure without extreme dehydration or loss of components present in the biomass.

This effect was further confirmed by the sol-gel transition point (G′ = G″), which represents the total collapse of the material's solid structure. Both hydrogels lost their elastic dominance at similar strain levels, with the transition occurring shortly before 174% strain for the 22 wt% sample and 159% for the 12 wt% sample. Interestingly, even after the structural collapse (at 174% strain), the 22 wt% hydrogel maintained a residual storage modulus (G′ ~ 119 Pa) significantly higher than that of the 12 wt% hydrogel (G′ ~ 6 Pa), in fact, starting from a higher biomass concentration contributed to a more consistent hydrogel, and in consequence, also higher residual modulus after collapsing. This indicates that while a higher biomass concentration does not necessarily delay the point of flow, it provides a much more robust, breakdown-resistant matrix, which is critical for maintaining some level of structural integrity under high shear conditions. This LVR (0.1% strain) was then used to perform the frequency sweep analysis (Figure 8).

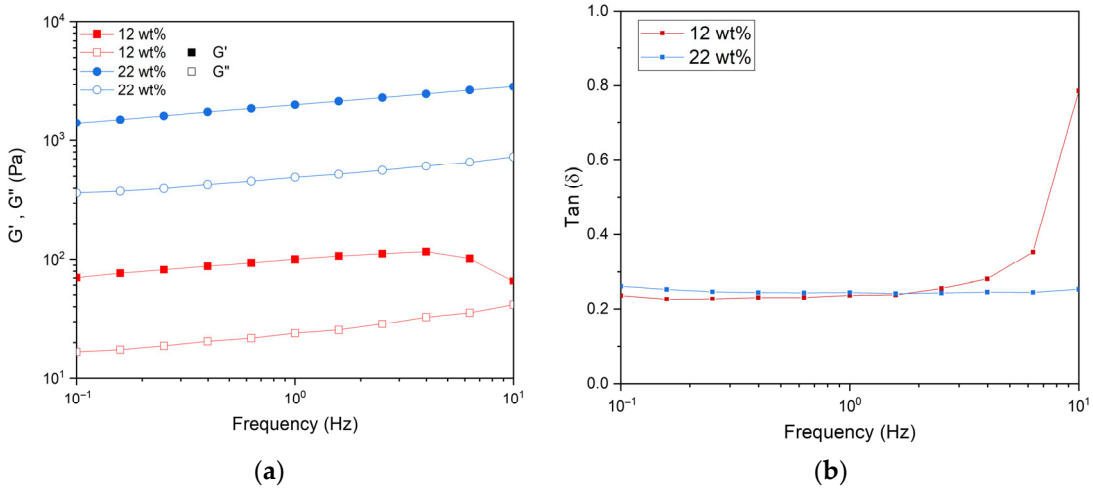

Figure 8. Frequency sweep test of SpB hydrogels (**a**): Elastic modulus (G′) and viscous modulus (G″), (**b**) loss factor (tan δ) of the hydrogels with 22 wt% and 12 wt% produced at pH 5.6.

The frequency sweep test, performed at a constant strain of 0.1% (a value established within the LVR), was used to evaluate the structural stability of the hydrogels over time and under varying oscillatory conditions (Figure 8). Throughout the studied frequency range (10^{-1} to 10^{1} Hz), the G′ was consistently higher than the G″ (G′ > G″) for both formulations. This confirms the predominant solid-like, viscoelastic gel characteristic of the materials.

As observed in the G′ values (Figure 8a), the 22 wt% hydrogel exhibited a modulus significantly higher than the 12 wt% hydrogel across the entire frequency range, confirming its superior structural rigidity due to the denser network formed by the higher biomass concentration. Furthermore, the loss factor (tan(δ)) (Figure 8b), calculated as the G″/G′ ratio, remained constant below unity (tan(δ) < 1) for both samples, with values around 0.25 (for 22 wt%) and 0.28 (for 12 wt%) in the range of 10^{-1} to 5 Hz. These low and stable values are characteristic of a predominantly elastic, solid-like material, confirming high structural integrity and stability. Although the moduli exhibit a slight frequency dependence, their low magnitudes ensure that the material's elastic character is dominant over the time scale of the measurements. These results align with previous reports on *L. platensis* biomass-residue bio-inks by Wang et al. [42], which also demonstrated stable, solid-like behaviour.

As described by authors like Kasapis & Bannikova [45], firm gels are characterized by moduli that are independent of frequency, whereas weak gels exhibit frequency-dependent moduli. Analysing Figure 8a, both the 12 wt% and 22 wt% hydrogels consistently maintained the relationship G′ > G″, confirming their stable, solid-like state. However, the G′ and G″ values displayed a slight but noticeable positive dependence on frequency (the slope is non-zero), indicating that the hydrogels, particularly the 22 wt% sample, align mechanically with the profile of a weak gel or a dense entangled system, where the network structure exhibits some time-dependent relaxation. Despite this frequency dependence, the 22 wt% hydrogel maintains significantly high structural properties. Consistent with the strain sweep results, its G′ average around 1900 Pa was significantly higher than that of the 12 wt% sample (approximately 97 Pa). This high G′ value, coupled with a relatively low and stable loss factor (tan(δ) around 0.25) (Figure 8b), confirms the structural integrity and elastic behaviour.

Therefore, while the material displayed a time-dependent relaxation profile consistent with a weak gel, it resulted in a sufficiently rigid material to ensure the potential stability and shape retention required for additive manufacturing applications. This sharp contrast is in stark contrast to truly fluid or dilute systems. However, its classification as a weak gel suggests that the material's successful processing will depend heavily on strict control of the applied shear rate during extrusion.

Comparing the frequency-sweep results with literature data, Sun et al. [44] reported G′ values of 800–1200 Pa using soy and potato protein isolates. However, to achieve these results, intensive ultrasound treatments and pH shifting were required to induce protein unfolding and subsequent gelation. The fact that the 22% SpB hydrogel produced in this study exhibits a higher G′ (ranging from 1400 to 2700 Pa for the optimized sample within the linear viscoelastic region) suggests that the use of integral biomass promotes synergistic interactions between endogenous proteins and polysaccharides. This demonstrates that an integral biomass 'zero-waste' approach can produce hydrogels with rheological properties compared to those made from isolated proteins, even without the need for high-energy treatments.

The recovery tests (Figure 9) were performed to evaluate the thixotropy and structural recovery of the hydrogels after exposure to high strain, accurately simulating the deposition and recovery cycles inherent to processing techniques such as 3D printing. The test executed three consecutive cycles, alternating between two low strain stages (0.1%, representing the LVR) and a high destructive strain (200%), a value set above the critical strain for both samples.

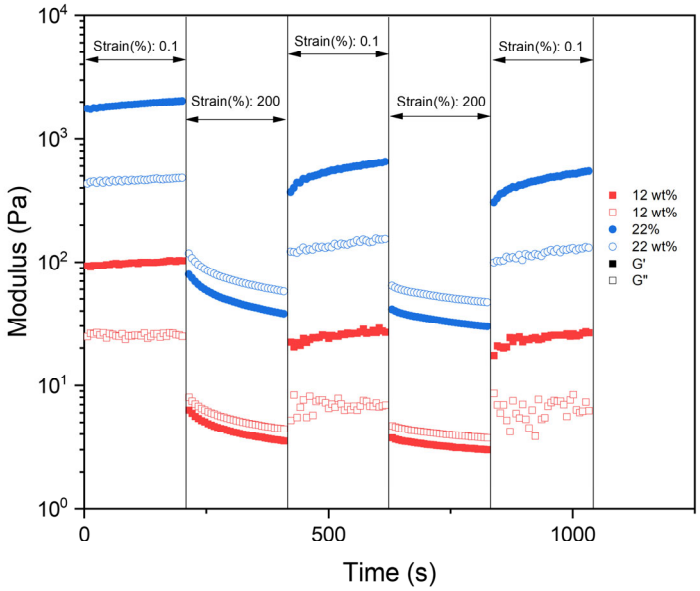

Figure 9. Modulus (G′ and G″) recovery test of SpB hydrogel with 22 wt% and 12 wt% produced at pH 5.6.

In the low-strain phase, both hydrogels consistently maintained the relationship G′ > G″, confirming their solid-like state. Consistent with the G′ values observed in the strain sweep and frequency sweep tests, the 22 wt% hydrogel showed a G′ approximately 24× higher than the 12 wt% hydrogel (initial G′ average 1900 Pa and 97 Pa), indicating significantly greater initial structural rigidity. Upon the application of the high strain (200%), both samples experienced a sudden reduction in both G′ and G″, confirming the necessary shear-thinning (pseudoplastic) behaviour observed in the flow test (Figure 6). This rapid transition is crucial for processability, as it enables the material to flow during extrusion.

Crucially, when the high-strain was removed, and the system returned to the low-strain region, both hydrogels demonstrated rapid thixotropic recovery, namely, G′ increased instantaneously. However, the quantitative analysis revealed a partial recovery of the original structure; in fact, the 22 wt% hydrogel recovered to an average G′ of approximately 515 Pa after the first cycle, corresponding to a 27.1% recovery of its initial G′. In comparison, the 12 wt% hydrogel recovered to an average G′ of approximately 25 Pa, demonstrating a similar recovery percentage of 25.8%.

Despite the partial recovery, the recovered G′ value of the 22 wt% sample (approximately 515 Pa) remained substantially higher than the initial G′ of the 12 wt% sample. The G′ > G″ after a destructive strain cycle confirms that the material retains sufficient mechanical integrity to maintain its shape and resist gravitational collapse (slumping) immediately after deposition, even after multiple cycles of structural breakdown.

2.5. 3D Printability Evaluation

Initially, a filament formation test was performed on the characterized samples. Only the optimized sample, at 22 wt% SpB, showed effective filament formation during extrusion, whereas the sample at 12 wt% biomass did not succeed due to its highly fluid characteristics. Consequently, the 22 wt% formulation was used for the printing tests.

Figure 10 illustrates the printability of the SpB hydrogel (22 wt% biomass, pH 5.6) as the bio-ink using two different extrusion methods: motor extrusion (a and b) and pneumatic extrusion (c and d). The 22 wt% formulation was selected for testing due to its superior rheological properties, specifically its high storage modulus (G′ approximately

1900 Pa) and excellent thixotropic recovery (approximately 27%), both critical to maintaining shape fidelity.

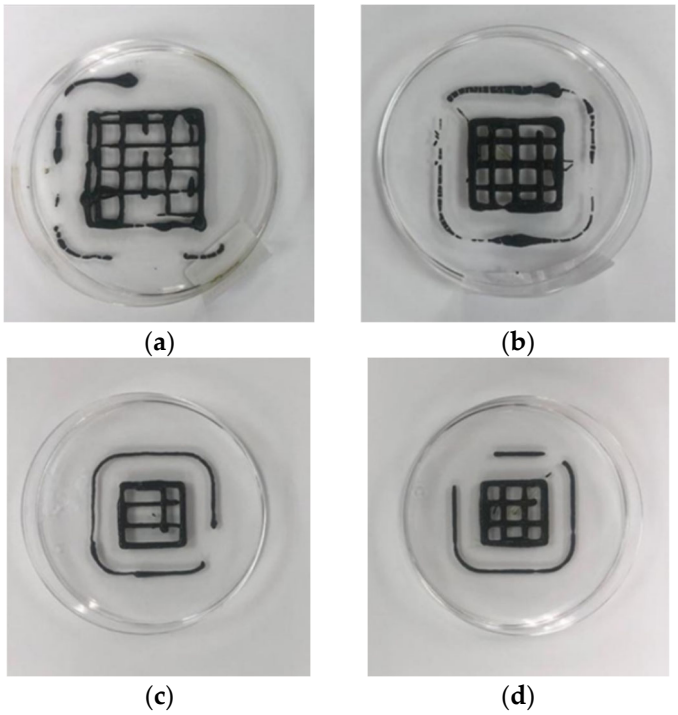

Figure 10. Printability of SpB hydrogel (22 wt% biomass, pH 5.6) by motor extrusion (**a**,**b**) and pneumatic extrusion (**c**,**d**).

Figure 10a,b show the printed mesh structures obtained via motor extrusion, a technique that allows for precise control over the flow rate independent of the materials' viscosity. The printing parameters used were a capillary diameter of 0.84 mm, a printing speed of 1 mm·s^{-1}, and a layer spacing of 1 mm.

Figure 10a, printed at a low flow rate of 55%, showed inconsistent filament deposition and structural failures, particularly at the corners, due to insufficient material output. The flow rate was too low relative to the printing speed, resulting in gaps and discontinuous filaments. The parameter was adjusted to a flow rate of 60% (Figure 10b), resulting in a significantly improved, complete mesh (Figure 10b). This fact indicates that while the hydrogel possesses the required structural strength (G′), successful printing depends on matching the material's shear-thinning characteristics with an adequate volumetric flow rate to ensure continuous, uniform extrusion.

Figure 10c,d show the pneumatic extrusion printing of the mesh structure, where material flow is controlled by applying air pressure. The parameters were set at a 1.2 mm syringe tip, a printing speed of 1 mm·s^{-1}, and a layer height of 1 mm. The pressure was manually adjusted to 0.8 bar to enable the material flow.

The hydrogel presented printing difficulties with the pneumatic system (Figure 10c,d) compared to motor extrusion. This limited printability is directly related to the system's rheological response. Manual control of pressure and the inherent mechanism of pneumatic extrusion make it challenging to maintain flow stability. The sudden pressure application leads to a high shear stress, resulting in a rapid, substantial drop in viscosity (as seen in the flow test, Figure 6). This high stress likely forces the material beyond its LVR and past its plateau viscosity, making the extruded filament overly fluid.

The superior results achieved by motor extrusion (Figure 10b) highlighted the necessity for precise control over shear rate and flow rate to adjust printing conditions and

the hydrogel's rheological properties, specifically its high modulus and its strong, but partial, recovery.

3. Materials and Methods

3.1. Samples and Reagents

The dried SpB was obtained from the local market Pingo Doce (Portugal, Bragança), and corresponds to a 100% Spirulina powder. Spirulina is the commercial name for the cyanobacterium *Limnospira platensis*, formerly classified as *Arthrospira platensis*. The sample, produced by Shine—SuperFoods (Setúbal, Portugal), presented the following characteristics: protein content 69 g/100 g; lipids 6.4 g/100 g, carbohydrates 4.4 g/100 g, and fibers 6.6 g/100 g. For pH adjustments, NaOH (purity $\geq$ 98%) purchased from Sigma-Aldrich (St. Louis, MO, USA), and acetic acid (purity $\geq$ 99.8%) purchased from Honeywell Fluka (Seelze, Germany) were used.

3.2. Hydrogel Forming Process

3.2.1. Initial Screening

To study the gel-forming process, biomass concentrations ranging from 2 to 20 wt% were evaluated. Each sample was subjected to a thermal treatment comprising heating to 85 °C and cooling to −4 °C for 24 h. Gelation ability was assessed using the inverted-tube test method. For this, a test tube containing the formulated sample was tilted to 90°. The sample was classified by flow behaviour: flowing samples were classified as solutions, and non-flowing samples as gels.

3.2.2. Sequential Design of Experiments

To evaluate the SpB's capacity to form gel, a sequential DoE (FFD 2^{6-2} and CCRD 2^2) was applied. This approach was chosen to reduce the number of experimental trials, thereby minimizing time and costs while still providing comprehensive information about the studied effects [46].

The FFD 2^{6-2} was initially applied to screen the six most relevant variables influencing the hydrogel formation (temperature, pH, heating time, stirring time, stirring speed, and biomass concentration). This design was followed by a CCRD 2^2, which was applied to maximize the effect of the two most relevant variables identified from the FFD (pH and biomass concentration).

The responses for all experimental runs and both designs were obtained from a TPA, specifically, firmness (y_1), consistency (y_2), cohesiveness (y_3), and work of cohesion (y_4). These TPA parameters were selected to characterize the mechanical properties relevant for hydrogel printability, with firmness (y_1) and cohesiveness (y_3) being crucial for structural integrity and shape retention after extrusion, while consistency (y_2) and work of cohesion (y_4) reflect the overall gel-forming capacity. The ranges of the studied variables for both experimental designs are presented in Table 3. For each experimental run, one sample was prepared, and the process repeatability was verified by conducting 3 replicates at the central point.

Hydrogels were prepared by suspending SpB in 100 mL of distilled water, according to the concentration levels specified in the experimental design. Before thermal treatment, the mixture was continuously stirred for approximately 12 h to ensure complete hydration of the biomass. After hydration, the sample pH was adjusted (according to the experimental design) and then subjected to mechanical treatment using an Ultraturrax CAT Scientific, Unidrive X1000D (Ballrechten-Dottingen, Germany) to disrupt the microalgal cell wall, facilitating the release of the gelling compounds (stirring rate and time defined by the experimental design). Subsequently, the sample was thermally treated in a water bath

(temperature and time defined by the experimental design). Finally, the resultant sample was transferred to a container and cooled for 24 h at 4 °C to complete the physical cross-linking and promote the hydrogel formation.

Table 3. Variables range applied in the fractional factorial design 2^{6-2} and in the central composite rotatable design 2^2.

Fractional Factorial Design (FFD) 2^{6-2}				
Variable	Symbol	Coded Variable Level		
		−1	0	1
Temperature (°C)	x_1	85	90	95
pH	x_2	6	8	10
Heating time (min)	x_3	30	45	60
Stirring time (min)	x_4	5	10	15
Stirring speed (rpm)	x_5	6500	8000	9500
Biomass concentration (wt%)	x_6	12	16	20

Central composite rotatable design (CCRD) 2^2						
Variable	Symbol	Coded Variable Level				
		−1.41	−1	0	1	1.41
pH	x_1	5.00	5.29	6.00	6.71	7.00
Biomass concentration (wt%)	x_2	16.00	16.87	19.00	21.13	22.00

3.3. Hydrogel Characterization

3.3.1. Texture Profile Analysis

The textural properties of the samples used as responses in the hydrogel-forming analysis were analysed in a texture analyser (Stable Micro Systems, TA. HDPlus Texture Analyser, Godalming, UK) according to the methodology described by Lupatini [32], with modifications. A cylindrical probe (A/BE−d35) was used, applying a compression distance of 40 mm and a test speed of 1 mm·s^{-1}. The following parameters were determined: firmness (maximum force required to deform the gel), consistency (describes the material's resistance to flow or deformation over time), cohesiveness (measures the force that holds the gel structure together, reflecting the material's ability to resist fragmentation) and the work of cohesion (total energy required to completely deform the gel, representing the total effort required to overcome and break the structure).

3.3.2. Syneresis Analysis

The syneresis analysis, corresponding to the percentage of water released from the gel network, followed the methodology described by Amaya-Llano et al. [47] was applied to the samples used for the optimization of the hydrogel formulation. Briefly, 1.5 g of the hydrogel sample was weighed and centrifuged at 2000 rpm for 30 min. The supernatant was carefully decanted, and the remaining sediment was weighed. The syneresis percentage was then determined according to Equation (5).

$$\text{Syneresis } (\%) = \frac{Initial\ mass - final\ mass}{initial\ mass} \times 100 \quad (5)$$

3.3.3. Hydrogel Microstructure

The morphology of the optimized hydrogel was examined using a scanning electron microscope (SEM, Phillips XL30, Eindhoven, The Netherlands) equipped with a tungsten filament, from lyophilized samples. The samples were coated with gold (Au) using an SC7640 High-Resolution Sputter Coater (Quorum Technologies, Newhaven, UK). The anal-

ysis conditions comprised an accelerating voltage of 25 kV in vacuum and a magnification range from 16× to 10^4×.

3.3.4. Rheological Analysis

The rheological behaviour of the optimized sample was evaluated using an AR-G2 rheometer (TA Instruments®, New Castle, DE, USA) at 25 °C with a 20 mm parallel plate geometry and a 1 mm gap. A non-hydrogel-forming sample was selected for comparison purposes. Viscosity measurements were initially performed by applying a continuous flow in the shear rate range from 10^{-3} to 10^3 s^{-1} to determine the flow curve. For oscillatory tests, an amplitude sweep (strain sweep) was conducted at a constant angular frequency of 1 Hz, with a shear strain ranging from 10^{-2}% up to 10^3%.

The LVR was determined as the region where the storage modulus (G′) remained constant. The critical strain (γc) was explicitly defined as the limit of the LVR, the strain at which the G′ dropped to 95% of its mean value within the LVR. Furthermore, the sol-gel transition point was identified as the strain where the storage modulus equalled the loss modulus (G′ = G″), marking the structural collapse.

Subsequently, a frequency sweep was performed within the LVR, with a constant strain of 0.1% and an angular frequency ranging from 10^{-2} to 10^2 Hz. Finally, a recovery test was executed at a constant frequency (1 Hz) using three alternating cycles of low strain (0.1%—rest) and high destructive strain (200%—stress) to assess the thixotropic structural recovery of the hydrogels.

3.4. 3D Printing Preliminary Analysis

The 3D printability of the optimized hydrogel formulation (22 wt% SpB at pH 5.6) was evaluated using a customized 3D bioprinter prototype. The system was configured to test the material using two distinct extrusion (motor and pneumatic) mechanisms to investigate the influence of shear control on print fidelity.

All tests were performed at a constant printing speed of 1 mm·s^{-1}. The effect of the capillary/nozzle diameter was investigated using two sizes: 0.84 mm and 1.2 mm. For the motor extrusion tests, the flow rate was systematically varied between 55% and 60% of the maximum capacity, aiming for optimal filament deposition. For the pneumatic extrusion setup, a manually adjusted pressure of 0.8 bar was applied to initiate and sustain the material flow.

3.5. Statistical Analysis

The experimental designs were analysed, and the response surface plots were generated by TIBCO Statistica 14.0 software (Statsoft Inc., Tulsa, OK, USA). Model adequacy was evaluated using the coefficient of determination (R^2) and the analysis of variance (ANOVA, F-test) for CCRD 2^2 at the 5% significance level (p-value ≤ 0.05). The significance of individual model terms (coefficients) in both FFD and CCRD was assessed using the Student's t-test (t). All experimental designs (FFD and CCRD) were performed at random.

4. Conclusions

This study demonstrated that the integral Spirulina biomass (22 wt%, pH 5.6) can be used to produce stable hydrogels with desirable structural, textural, and rheological properties. The optimized hydrogel exhibited low syneresis, a favourable internal microstructure, solid-like behaviour with a storage modulus (G′) ~1890 and loss factor (tan (δ)) < 0.3, shear-thinning properties, and high resistance to structural failure. Preliminary 3D printing tests confirmed its suitability for forming controlled mesh structures. These findings highlight the potential of *S. platensis* integral biomass as a high-value ingre-

dient for innovative food applications and provide a foundation for further research on microalgae-based hydrogel systems.

Supplementary Materials: The following supporting information can be downloaded at https://www.mdpi.com/article/10.3390/molecules31040591/s1. Table S1: Effect of the studied variables (x_1–x_6) on texture responses; Table S2: Analysis of Variance for the firmness (g), consistency (g·s), cohesiveness (g), and work of cohesion (g·s) responses of fractional factorial design (FFD) 2^{6-2}; Table S3: Analysis of Variance (percentage of the explained variance (R^2), $F_{calculated}$ and $F_{tabulated}$ values) for the firmness (g), consistency (g·s), cohesiveness (g), and work of cohesion (g·s) responses; Table S4: Regression coefficients estimated for the models of firmness (g), consistency (g·s), cohesiveness (g), and work of cohesion (g·s) from the CCRD 2^2 results.

Author Contributions: Conceptualization: L.L.A., M.F.B., A.S.-E. and E.C.; Methodology: L.L.A., S.C.S.-P., A.H.-S., E.C.R. and R.H.; Investigation: L.L.A., S.C.S.-P., A.H.-S., E.C.R. and A.S.-E.; Resources: E.C.R., R.H. and M.F.B.; Data curation: L.L.A.; Writing—original draft preparation, L.L.A.; Writing—review and editing, R.H., A.S.-E., E.C.R., E.C. and M.F.B.; Supervision, R.H., A.S.-E., E.C. and M.F.B. All authors have read and agreed to the published version of the manuscript.

Funding: We acknowledge the Foundation for Science and Technology (FCT, Portugal) for financial support through national funds FCT/MCTES (PIDDAC) to CIMO UID/00690/2025 (10.54499/UID/00690/2025) and UID/PRR/00690/2025 (10.54499/UID/PRR/00690/2025) and SusTEC LA/P/0007/2020 (10.54499/LA/P/0007/2020); national funding by FCT, I.P., through the institutional scientific employment program contract of A. Santamaria-Echart; FCT for the PhD research grant of Samara C. Silva-Pituco (SFRH/BD/148281/2019, DOI: 10.54499/SFRH/BD/148281/2019); and the Ibero-American Programme for Science and Technology for Development (CYTED) through Project 124RT0164 (INNOPROT).

Data Availability Statement: Data will be made available upon request.

Conflicts of Interest: The authors declare no conflicts of interest.

References

1. Aiking, H.; de Boer, J. The next Protein Transition. *Trends Food Sci. Technol.* **2020**, *105*, 515–522. [CrossRef]
2. Williamson, E.; Ross, I.L.; Wall, B.T.; Hankamer, B. Microalgae: Potential Novel Protein for Sustainable Human Nutrition. *Trends Plant Sci.* **2024**, *29*, 370–382. [CrossRef] [PubMed]
3. Blanco-Llamero, C.; García-García, P.; Señoráns, F.J. An Integrated Biorefinery Process to Revalorize Marine Biomass from the Microalga Nannochloropsis Gaditana Using Pressurized Green Solvents. *Mar. Drugs* **2025**, *23*, 263. [CrossRef] [PubMed]
4. de Souza Silva, P.H.B.; Degli Esposti, G.; Ndiaye, N.C.G.; Pedro, G.A.; Maass, D. Microalgae for Brewery Wastewater Treatment and Biomass Valorization: A Systematic Review. *Environ. Sci. Pollut. Res.* **2025**, *2025*, 1–17. [CrossRef]
5. Santos, B.; Freitas, F.; Sobral, A.J.F.N.; Encarnação, T. Microalgae and Circular Economy: Unlocking Waste to Resource Pathways for Sustainable Development. *Int. J. Sustain. Eng.* **2025**, *18*, 2501488. [CrossRef]
6. Zhang, Z.; Lei, D.; Yang, J.; Liu, Z. Microalgae Biorefinery in the Belt and Road Initiative: Opportunities for Green Growth. *Bioresour. Technol.* **2026**, *440*, 133428. [CrossRef]
7. Thoré, E.S.J.; Muylaert, K.; Bertram, M.G.; Brodin, T. Microalgae. *Curr. Biol.* **2023**, *33*, R91–R95. [CrossRef]
8. Gul, S.; Shahnaz, L.; Raiz, S.; Nawaz, M.F. Microalgae: Production, Consumption and Challenges. In *Algae as a Natural Solution for Challenges in Water-Food-Energy Nexus: Toward Carbon Neutrality*; Springer Nature: Singapore, 2024; pp. 31–59. [CrossRef]
9. De Obeso Fernandez Del Valle, A.; Scheckhuber, C.Q. From Past to Present: Biotechnology in Mexico Using Algae and Fungi. *Plants* **2021**, *10*, 2530. [CrossRef]
10. de Morais, M.G.; Colla, L.M.; Costa, J.A.V. Microalgae Superfoods. In *Microalgal Bioengineering*; Springer International Publishing: Cham, Switzerland, 2024; pp. 281–294. [CrossRef]
11. Sun, H.; Wang, Y.; He, Y.; Liu, B.; Mou, H.; Chen, F.; Yang, S. Microalgae-Derived Pigments for the Food Industry. *Mar. Drugs* **2023**, *21*, 82. [CrossRef] [PubMed]
12. Ng, H.-S.; Chew, L.-L. Valuable Compounds Produced by Microalgae. In *Handbook of Biorefinery Research and Technology: Production of Biofuels and Biochemicals*; Springer Nature: Singapore, 2024; pp. 731–749. [CrossRef]
13. Vieira, V.V.; Benemann, J.; Vonshak, A.; Belay, A.; Ras, M.; Unamunzaga, C.; Cadoret, J.P.; Rizzo, A. Spirulina in the 21st Century: Five Reasons for Success in Europe. *J. Appl. Phycol.* **2025**, *37*, 2203–2216. [CrossRef]

14. Prates, J.A.M. Unlocking the Functional and Nutritional Potential of Microalgae Proteins in Food Systems: A Narrative Review. *Foods* **2025**, *14*, 1524. [CrossRef]
15. Sotiroudis, T.G.; Sotiroudis, G.T. Health Aspects of Spirulina (Arthrospira) Microalga Food Supplement. *J. Serbian Chem. Soc.* **2013**, *78*, 395–405. [CrossRef]
16. Becker, E.W. Micro-Algae as a Source of Protein. *Biotechnol. Adv.* **2007**, *25*, 207–210. [CrossRef] [PubMed]
17. Torres-Tiji, Y.; Fields, F.J.; Mayfield, S.P. Microalgae as a Future Food Source. *Biotechnol. Adv.* **2020**, *41*, 107536. [CrossRef]
18. López-Rodríguez, A.; Mayorga, J.; Flaig, D.; Fuentes, G.; Cotabarren, J.; Obregón, W.D.; Gómez, P.I. Comparison of Two Strains of the Edible Cyanobacteria Arthrospira: Biochemical Characterization and Antioxidant Properties. *Food Biosci.* **2021**, *42*, 101144. [CrossRef]
19. Bernaerts, T.M.M.; Gheysen, L.; Foubert, I.; Hendrickx, M.E.; Van Loey, A.M. The Potential of Microalgae and Their Biopolymers as Structuring Ingredients in Food: A Review. *Biotechnol. Adv.* **2019**, *37*, 107419. [CrossRef] [PubMed]
20. Yi, X.; Xie, J.; Mei, J. Recent Advances in Marine-Derived Polysaccharide Hydrogels: Innovative Applications and Challenges in Emerging Food Fields. *Polymers* **2025**, *17*, 2553. [CrossRef]
21. Li, C.; Du, M.; Han, Y.; Sun, W.; Chen, Z.; Liu, Q.; Zhu, H.; Zhao, L.; Li, S.; Wang, J. Microalgae in Health Care and Functional Foods: β-Glucan Applications, Innovations in Drug Delivery and Synthetic Biology. *Front. Pharmacol.* **2025**, *16*, 1557298. [CrossRef]
22. Terpou, A.; Dahiya, D.; Nigam, P.S. Prospects of Gels for Food Applications from Marine Sources: Exploring Microalgae. *Gels* **2025**, *11*, 569. [CrossRef]
23. Guil-Guerrero, J.L.; Prates, J.A.M. Microalgae Bioactives for Functional Food Innovation and Health Promotion. *Foods* **2025**, *14*, 2122. [CrossRef]
24. Ozorio, L.; Passerini, A.B.S.; da Silva, A.P.C.; Braga, A.R.C.; Perrechil, F. Designing Plant-Based Foods: Biopolymer Gelation for Enhanced Texture and Functionality. *Foods* **2025**, *14*, 1645. [CrossRef]
25. Pipliya, S.; Kumar, S.; Gupta, R.K.; Das, R.S.; Meena, D.; Srivastav, P.P.; Tiwari, B.K.; Garcia-Vaquero, M. The Future of Algal Proteins: Innovations in Extraction and Modifications, Functional Properties, and Sustainable Food Applications. *Future Foods* **2025**, *11*, 100549. [CrossRef]
26. Sampaio, U.M.; Siqueira, K.F.; Starling, C.A.; Araújo, F.I.R.O. Aspectos Gerais de Cultivo, Métodos de Secagem e Características Da Cianobacteria Spirulina Platensis. *Rev. Process. Químicos* **2016**, *10*, 133–143. [CrossRef]
27. Benelhadj, S.; Douiri, S.; Ghouilli, A.; Hassen, R.B.; Keshk, S.M.A.S.; El-kott, A.; Attia, H.; Ghorbel, D. Extraction of Arthrospira Platensis (Spirulina) Proteins via Osborne Sequential Procedure: Structural and Functional Characterizations. *J. Food Compos. Anal.* **2023**, *115*, 104984. [CrossRef]
28. Bertsch, P.; Böcker, L.; Mathys, A.; Fischer, P. Proteins from Microalgae for the Stabilization of Fluid Interfaces, Emulsions, and Foams. *Trends Food Sci. Technol.* **2021**, *108*, 326–342. [CrossRef]
29. da Silva Faresin, L.; Devos, R.J.B.; Reinehr, C.O.; Colla, L.M. Development of Ice Cream with Reduction of Sugar and Fat by the Addition of Inulin, Spirulina Platensis or Phycocyanin. *Int. J. Gastron. Food Sci.* **2022**, *27*, 100445. [CrossRef]
30. Dinçoğlu, A.H.; Akça, S.S.; Çalışkan, Z. Effect of Spirulina Platensis on Probiotic, Nutritional, and Quality Properties of Yogurt. *Int. Food Res. J.* **2024**, *31*, 157. [CrossRef]
31. Ismail, H.A.; El-Sawah, T.H.; Ayyash, M.; Adhikari, B.; Elkot, W.F. Functionalization of Ricotta Cheese with Powder of Spirulina Platensis: Physicochemical, Sensory, and Microbiological Properties. *Int. J. Food Prop.* **2023**, *26*, 1968–1983. [CrossRef]
32. Nitsos, C.; Filali, R.; Taidi, B.; Lemaire, J. Current and Novel Approaches to Downstream Processing of Microalgae: A Review. *Biotechnol. Adv.* **2020**, *45*, 107650. [CrossRef]
33. Piyatilleke, S.; Thevarajah, B.; Nimarshana, P.H.V.; Ariyadasa, T.U. Microalgal Biofuels: Challenges and Prospective in the Framework of Circular Bioeconomy. *Energy Nexus* **2025**, *17*, 100338. [CrossRef]
34. Lafarga, T.; Fernández-Sevilla, J.M.; González-López, C.; Acién-Fernández, F.G. Spirulina for the Food and Functional Food Industries. *Food Res. Int.* **2020**, *137*, 109356. [CrossRef]
35. Ezhumalai, G.; Arun, M.; Manavalan, A.; Rajkumar, R.; Heese, K. A Holistic Approach to Circular Bioeconomy Through the Sustainable Utilization of Microalgal Biomass for Biofuel and Other Value-Added Products. *Microb. Ecol.* **2024**, *87*, 61. [CrossRef]
36. Yu, C.; Chen, L.; Xu, M.; Ouyang, K.; Chen, H.; Lin, S.; Wang, W. The Effect of PH and Heating on the Aggregation Behavior and Gel Properties of Beef Myosin. *LWT* **2024**, *191*, 115615. [CrossRef]
37. Hydrogel, D.; Roca-Arroyo, A.F.; Gutierrez-Rivera, J.A.; Morton, L.D.; Castilla-Casadiego, D.A. Hydrogel Network Architecture Design Space: Impact on Mechanical and Viscoelastic Properties. *Gels* **2025**, *11*, 588. [CrossRef]
38. Wu, Q.; Buijs, J.; de Groot, S.; van der Kooij, H.M.; van der Gucht, J.; Kodger, T.E. Spatially Heterogenous Dynamics in Colloidal Gels during Syneresis. *Soft Matter* **2023**, *19*, 5336–5344. [CrossRef]
39. Qi, X.; Li, Y.; Xiao, J.; Shen, L.; He, Z.; Xie, J. Reinforcing the Pea Protein Isolate-Gellan Gum Composite Gels by PH-Shifting Pretreatment: Emphasizing PH-Modulated Aggregation Behavior and Gelation Mechanisms. *Food Struct.* **2025**, *46*, 100481. [CrossRef]

40. Wang, Y.; Zhao, J.; Zhang, W.; Liu, C.; Jauregi, P.; Huang, M. Modification of Heat-Induced Whey Protein Gels by Basic Amino Acids. *Food Hydrocoll.* **2020**, *100*, 105397. [CrossRef]
41. Bercea, M. Rheology as a Tool for Fine-Tuning the Properties of Printable Bioinspired Gels. *Molecules* **2023**, *28*, 2766. [CrossRef] [PubMed]
42. Wang, M.; Lu, X.; Zheng, X.; Li, W.; Wang, L.; Qian, Y.; Zeng, M. Rheological and Physicochemical Properties of Spirulina Platensis Residues-Based Inks for Extrusion 3D Food Printing. *Food Res. Int.* **2023**, *169*, 112823. [CrossRef]
43. Zhao, L.; Wang, K.; Zhu, J.; Guo, J.; Hu, Z. Temperature-Induced Interaction with Carboxymethyl Cellulose Affected the Rheological Properties and Structure of Wheat Gluten. *LWT* **2020**, *133*, 109993. [CrossRef]
44. Sun, Y.; Wang, L.; Wang, H.; Zhou, B.; Jiang, L.; Zhu, X. Effect of PH-Shifting and Ultrasound on Soy/Potato Protein Structure and Gelation. *Food Hydrocoll.* **2025**, *159*, 110672. [CrossRef]
45. Kasapis, S.; Bannikova, A. Rheology and Food Microstructure. In *Advances in Food Rheology and Its Applications*; Woodhead Publishing: New Delhi, India, 2017; pp. 7–46. [CrossRef]
46. Rodrigues, M.I.; Iemma, A.F. *Experimental Design and Process Optimization*; Crc Press: Boca Raton, FL, USA, 2014; pp. 1–304. [CrossRef]
47. Amaya-Llano, S.L.; Martínez-Alegría, A.L.; Zazueta-Morales, J.J.; Martínez-Bustos, F. Acid Thinned Jicama and Maize Starches as Fat Substitute in Stirred Yogurt. *LWT* **2008**, *41*, 1274–1281. [CrossRef]